Title: Immunodominant surface epitopes power immune evasion in the African trypanosome

Authors: Anastasia Gkeka[1,2,8], Francisco Aresta-Branco[1,3,8], Gianna Triller[1], Evi P. Vlachou[1], Mirjana Lilic[4], Paul Dominic B. Olinares[5], Kathryn Perez[6], Brian T. Chait[5], Renata Blatnik[7], Thomas Ruppert[7], C. Erec Stebbins[3,*], F. Nina Papavasiliou[1,9,*]

Affiliations:

[1]Division of Immune Diversity, German Cancer Research Center, Heidelberg, 69120, Germany.

[2]Faculty of Biosciences, University of Heidelberg, Heidelberg, 69120, Germany.

[3]Division of Structural Biology of Infection and Immunity, German Cancer Research Center, Heidelberg, 69120, Germany.

[4]The Rockefeller University, Laboratory of Structural Microbiology, New York, NY, 10065, USA.

[5]The Rockefeller University, Laboratory of Mass Spectrometry And Gaseous Ion Chemistry, New York, NY, 10065, USA.

[6]Protein Expression and Purification Core Facility, EMBL Heidelberg, Heidelberg, 69117, Germany.

[7]Center for Molecular Biology of Heidelberg University, DKFZ-ZMBH Alliance, Heidelberg, 69120, Germany.

[8]These authors contributed equally.

[9]Lead contact

*Correspondence to: n.papavasiliou@dkfz-heidelberg.de, e.stebbins@dkfz-heidelberg.de

Abstract

The African trypanosome survives the immune response of its mammalian host by antigenic variation of its major surface antigen (the Variable Surface Glycoprotein, or VSG). Here we describe the antibody repertoires elicited by different VSGs. We show that the repertoires are highly restricted, and are directed predominantly to distinct epitopes on the surface of the VSGs. They are also highly discriminatory: minor alterations within these exposed epitopes confer antigenically-distinct properties to these VSGs and elicit different repertoires. We propose that the patterned and repetitive nature of the VSG coat focuses host immunity to a restricted set of immunodominant epitopes per VSG, eliciting a highly stereotyped response, minimizing cross reactivity between different VSGs and facilitating prolonged immune evasion through epitope variation.

Keywords

African trypanosome, host-pathogen interactions, Variant Surface Glycoproteins, antigenic variation, immune evasion, immunogenic epitopes, immunodominance, antibody repertoires, post-translational modifications

42 **Introduction**

43 The African trypanosome (*Trypanosoma brucei spp*) is a strictly extracellular parasite,
44 infection with which elicits a robust antibody response against its Variant Surface Glycoprotein
45 (VSG) coat (Stijlemans et al., 2017; Verdi and Zipkin et al., 2020). This response mediates
46 parasite clearance, but is vulnerable to immune escape from variants that have switched surface
47 coat composition (Mugnier et al., 2015). The VSG protein consists of a large N-terminal domain
48 (NTD, approximately 350 amino acids) and a shorter C-terminal domain (CTD, approximately
49 100 amino acids), the latter being linked to the membrane via a GPI anchor (Grünfelder et al.,
50 2002). It is speculated that the majority of immune epitopes are located on the tope lobe of the
51 NTD, which is highly accessible to the immune system, however there are no antibody-VSG
52 co-crystal structures available to support this hypothesis (Aresta-Branco and Erben et al., 2019;
53 Bangs, 2018; Zoll et al., 2018), and recent studies have challenged this model (Hempelmann et
54 al., 2021).

55 The dynamic interplay between VSG-coat-switching by trypanosomes and the B cell
56 response of the host that they evade is central to the maintenance of chronic infection (Silva-
57 Barrios et al., 2018). Nonetheless, very little is known about the nature of the antibody response
58 against the VSG coat. A small number of papers dating back to the 1990s revealed that acute
59 infection with *T. brucei* leads to extraordinarily high levels of IgM in humans and in mice
60 (Verdi and Zipkin et al., 2020). The antibody response has often been characterized as
61 polyclonal and many of those antibodies are autoreactive (Diffley, 1983; Müller et al., 1996;
62 Verdi and Zipkin et al., 2020). However, these data are conceptualized in the context of a
63 prolonged infection that itself is polyclonal in VSG-archetype. An understanding of the
64 response to individual VSG variants in a controlled setting is therefore lacking, since the
65 culmination of multiple separate responses to different VSGs would produce a "polyclonal" B
66 cell output in the greater infection context. Importantly, immunization or exposure to specific
67 VSG surface coats prevents later infection by cells expressing that same coat, indicating that

68 coat-specific antibodies are produced during infection (Campbell et al., 1977; Mugnier et al.,
69 2015).

70 In order to explore the parameters of the antibody response to *T. brucei*, we examined the
71 antibody repertoires elicited by two specific VSGs. These were chosen to broadly represent the
72 two primary VSG "classes": VSG2 (a Class-A VSG) and VSG3 (a Class-B VSG) (Carrington
73 et al., 1991). Herein, we demonstrate that the repertoires show restricted V-gene usage which
74 is highly reproducible between animals and experiments. Moreover, we show that small
75 alterations (e.g., point mutations) within VSG surfaces result in distinct repertoires, suggesting
76 that antibodies elicited by VSGs are selective toward specific epitopes on the surface of each
77 VSG, and can discriminate even between single amino acid changes. We speculate that this
78 intense immune-focusing of antibody responses to a very small number of epitopes per VSG
79 may have evolved to reduce cross-reactivity between VSGs and to facilitate prolonged immune
80 evasion.

81

82 **Results**

83 **Trypanosome infections lead to rapid plasma cell expansion**

84 To generate the antibody repertoires, we infected animals with each specific VSG-
85 expressing parasite, and either "cleared" the parasites with the anti-protozoan compound
86 diminazene four days after infection (as infection is often rapidly lethal) (Pinger et al., 2017) or
87 allowed the animals to clear the trypanosomes naturally (whenever feasible) after the first peak
88 of parasitemia (at which point the parasites that have switched VSG coats remain and seed the
89 next peak of parasitemia). Initial analyses of infected C57BL/6 mice showed a robust expansion
90 of plasma cells (Figure 1A, Figure S1A). This expansion was common to all infections
91 regardless of whether parasites were cleared by the animals (usually by day 6 or day 7 post
92 infection) or whether they were pharmacologically cleared earlier with diminazene (days 4 and

93 5), allowing for the maturation of the antibody response until collection (which was uniformly
94 at day 8 post infection – Figure 1B). This is also consistent with known parameters of disease
95 progression (Black et al., 1985; Jayaraman et al., 2019; Mugnier et al., 2015).

96 Typically, the characterization of an antigen-specific antibody repertoire benefits from the
97 "baiting" of antigen specific B cells using the antigen itself conjugated to a fluorophore (PE or
98 APC) (Scheid et al., 2009; Tiller et al., 2008). However, plasma cells are notoriously hard to
99 bait as they downregulate surface expression of Ig and rather secrete the vast majority of the
100 antibody they produce, so that very little antibody remains surface-bound and accessible. We
101 therefore proceeded to sort all plasma cells according to surface marker expression
102 (CD138+/CD19^{lo}) (Pracht et al., 2017) into 384-well plates. The antibody repertoire of plasma
103 cells was then assembled after two rounds of single cell PCR and paired heavy (IgH) and light
104 (Igκ/λ) gene sequence analysis (Tiller et al., 2008).

105

106 **The VSG2$_{WT}$ repertoire is characterized by a small number of heavy and light chain**
107 **variable region genes**

108 We first focused on the repertoire elicited by VSG2-coated parasites. Surprisingly for a
109 non-baited repertoire, plasma cells elicited from mice infected with VSG2 were dominated by
110 cells carrying only four VH+VL chain pairings (VH10.1 or VH10.3 with VL19-20 or VL19-
111 14, Figure 1C). These combinations, which are absent in naïve mice (Figure S1B), formed the
112 plurality of the repertoire when mice were pharmacologically treated to remove trypanosomes
113 four days after infection, but they became increasingly prevalent in repertoires of animals that
114 cleared trypanosomes naturally a day before collection, and even more dominant in repertoires
115 of animals that cleared the infection the day we collected plasma cells (Figure 1C). This
116 suggests a rapid and robust response to the parasite, stereotyped and highly reproducible
117 between mice, that may become increasingly diversified as more antigens become available
118 after parasite lysis.

119 We reasoned that the repertoire we collected closest to natural clearance would contain the
120 B cells likely expressing the most potent anti-coat-specific antibodies and proceeded to analyze
121 it further. While dominated by cells expressing two distinct immunoglobulin (Ig) heavy and Ig
122 light chain gene pairs, the B cells elicited by VSG2-coated *T. brucei* were not monoclonal: each
123 VH10 heavy and 19-20 or 19-14 light chain V region was joined to a set of DJ or J gene
124 segments representing a wide swath of CDR3 variants (Figure 1D). This lack of clonal
125 expansion is also evident from the Shannon entropy index, which is a statistical sequence-based
126 measure of clonality (Figure 1C, bottom of each circos plot).

127 We therefore picked a small number of heavy and light chain pairs from the
128 overrepresented V gene segments identified and proceeded to express them recombinantly as
129 soluble antibodies in 293T cells. Indeed, 7 out of 11 of these antibodies are capable of binding
130 live, VSG2-coated *T. brucei*, but not parasite cells coated with a different VSG protein (Figure
131 1D, Figure 3C). Antibodies that did not use these V segments were not able to bind VSG2-
132 coated parasites (Figure S2). We conclude that the VSG2-elicited plasma cell repertoire
133 represents an oligoclonal expansion primarily of four variable region defined pairs, which are
134 mostly unmutated (Figure 1D). The V gene signature that defines this repertoire is stereotyped
135 between mice (Figure 1C), suggesting both that the VSG2-specific paratope is likely located
136 within highly-specific variable regions of the antibody protein, and that these antibodies are
137 likely generated against a common immunodominant epitope.

138

139 **The structure of VSG2$_{WT}$ contains a calcium binding pocket, which defines the**
140 **immunodominant epitope**

141 Epitope identification is often achieved by structural analyses of repertoire-defined
142 antibodies together with the antigen that elicited them (Triller et al., 2017). We therefore sought
143 to crystallize VSG2 (specifically, the larger, surface-exposed N-terminal domain of the VSG,
144 or "NTD") together with VSG2-specific Fab-fragments. All crystals obtained were of VSG2

145 alone, however (Figure S3C, Table S1), likely because most antibodies elicited by *T. brucei*
146 infection are of the IgM isotype (Figure S4, A and B) (Verdi and Zipkin et al., 2020) and are
147 likely of low affinity (but high avidity). These antibodies are thus unlikely to bind with high-
148 affinity when produced recombinantly as an IgG (or Fab) fragment (as current methods for the
149 recombinant production of pentameric IgM are poorly optimized). Serendipitously, the crystals
150 did allow us to re-solve the structure of VSG2 to much higher resolution compared to previous
151 work (Freymann et al., 1990; Metcalf et al., 1987), with unexpected findings. The protein
152 structure of VSG2 from these new crystals is nearly identical to that from the 1990 crystal form,
153 with a root-mean-square deviation of 0.87Å over 1420 atoms of a monomer in the dimer (Figure
154 2A, Figure S3A). However, in later stages of model refinement, unusually large electron density
155 around solvent molecules was modeled effectively with calcium (Figure 2, B and C), an ion not
156 present in older structures likely due to the use of chelating agents in the purification from
157 animal blood (Cross, 1975, 1984). Calcium is octahedrally coordinated in VSG2 through a
158 network of oxygen bonds: four from three consecutive amino acid side-chains at the end of a
159 β-strand (bidentate-D208, N209, and D210, henceforth the "DND motif"), the carbonyl-oxygen
160 from G155 in an opposing loop, and three water molecules in the solvent shell above the protein
161 (each water coordinated by other side-chain and main-chain contacts from the protein, Figure
162 2C).

163 There is little change in the fold or amino acid side-chain positioning between the calcium
164 bound and free structures of VSG2 (Figure 2, A-C), indicating that the pocket does not undergo
165 any significant conformational changes upon calcium binding. The presence of calcium was
166 verified both by mass spectrometry as well as isothermal titration calorimetry (Figure S5, A-
167 D). The calcium binding pocket in VSG2 appears to be unique, not closely resembling any
168 published structures in the PDB (e.g., DALI homology search) (Holm, 2020). The pocket
169 occurs near the "top" of the NTD of VSG2, slightly sheltered from the uppermost surface
170 (Figure 2A). A triple mutation of the DND motif to alanine ($VSG2_{AAA}$) abrogates calcium

171 binding (Figure S5, E-G) without any significant conformational changes (Figure 2, A and C,
172 Figure S3, A and D), although electrostatic surfaces generated from the three structures show
173 an expected change to a more neutral charge distribution in the pocket region of the mutant
174 (Figure 3A).

175 Unexpectedly, despite the high similarity between the wild type and mutant structures,
176 antisera elicited by infection with $VSG2_{WT}$ coated trypanosomes do not bind trypanosomes
177 expressing the minor variant represented by the $VSG2_{AAA}$ mutant (Figure 3B). Furthermore,
178 our recombinantly expressed antibodies specific to the $VSG2_{WT}$ coat were unable to bind the
179 $VSG2_{AAA}$ mutant coat (Figure 3C, Figure S2), despite the fact that these mutations did not cause
180 conformational changes in VSG2 (Figure 2, A and C, Figure S3A). This suggests that the VSG2
181 epitope recognized by both antisera and monoclonal antibodies is located within the region
182 defined by the DND motif and conversely, that antibodies to VSG2-coated trypanosomes are
183 capable of a high degree of epitope discrimination.

184

185 **The $VSG3_{S317A}$ repertoire is defined by a signature light chain V gene (gn33), absent from**
186 **the wild type**

187 To assess whether this combination of epitope immunodominance and antibody
188 discrimination characterizes the epitope space of other VSGs, we analyzed antibody repertoires
189 from plasma cells collected from animals infected with VSG3-coated trypanosomes. VSG3 is
190 a member of a different VSG class with significant structural and post-translational
191 modifications distinguishing it from VSG2 (Class A vs Class B VSGs, respectively)
192 (Carrington et al., 1991). Previously, we had solved the crystal structure of the VSG3 NTD,
193 leading to the unexpected identification of an *O*-linked glycosylation of a serine residue (S317,
194 heterogeneously modified with 0-3 hexose residues) located in the center of the top surface of
195 the protein (Pinger, Nešić and Ali, et al., 2018). Mutation of that serine to an alanine residue
196 ablated glycosylation, reduced parasite virulence, and enhanced the effectiveness of the host

197 immune response (Pinger, Nešić and Ali, et al., 2018). At the time we hypothesized that this
198 was due to the tendency of *O*-linked sugars to adopt multiple conformational states (Lisowska,
199 2002), thus further diversifying the epitope space of the VSG3 coat. Therefore, to assess
200 whether VSG3 coated trypanosomes lacking this post-translational modification could also
201 elicit a stereotyped immune response toward an immunodominant epitope (such as we have
202 seen for VSG2-coated parasites), we first infected mice with S317A mutant parasites
203 ($VSG3_{S317A}$), and analyzed the resulting plasma cell antibody responses either after natural
204 clearance or after treatment with diminazene. As was the case for VSG2 coated parasites,
205 $VSG3_{S317A}$ coated parasites were also capable of reproducibly eliciting a restricted B cell
206 repertoire in multiple distinct infections (Figure 4A). However, this repertoire was now defined
207 by a major light chain V gene (VL-gn33) pairing with a larger number of heavy chains (Figure
208 4A). Again, recombinant expression of a number of these heavy and light chain pairs as secreted
209 IgG1s in 293T cells show that many of the antibodies elicited by $VSG3_{S317A}$ coats are capable
210 of binding their cognate parasites (Figure 4, B and C, Figure S6, A and B). Although the
211 common light chain variable gene (gn33) is clearly important for binding, the proper heavy
212 chain is also necessary, since pairing of the gn33 light chain with a different VH can result in a
213 loss of binding (Figure S6, C and D). Whether the common light chain plays a role in increasing
214 antibody binding to the repetitive coat remains to be investigated.

215 We also analyzed the resulting plasma cell response after infection with $VSG3_{WT}$ followed
216 by treatment with diminazene (as the high virulence of the strain is incompatible with natural
217 clearance). We found that the light-chain restriction seen with $VSG3_{S317A}$ elicited repertoires is
218 now entirely abolished, strongly suggesting that the addition of up to 3 *O*-linked hexoses per
219 VSG3 molecule functions to diversify the presumed immunodominant epitope presented by the
220 $VSG3_{S317A}$ coated parasite (Figure 4D). Furthermore, the addition of sugars entirely prevented
221 the major VL (gn33) carrying antibody pairs from binding $VSG3_{WT}$ coated parasites (Figure 4,
222 B and C), suggesting that antibodies elicited to the parasite coat are focused near-exclusively

223 on the epitope that contains the *O*-linked hexoses. Conversely, of the four antibodies we
224 reconstituted and tested that were elicited by the wildtype ($VSG3_{WT}$) infection, three were able
225 to bind the sugarless coat, and one was selective to the sugar on S317 (capable only of binding
226 the wildtype) (Figure 4, B and C).

227

228 **The anti-VSG3 repertoire is highly sensitive to a prominent immunodominant epitope on**
229 **the surface of VSG3**

230 A comparison of mutant and wild type structures verified that the protein surface
231 between the two VSG3 variants was identical (Figure 5A) but yielded a surprise in the form of
232 an additional sugar in a neighboring serine (S319). We confirmed this in the $VSG3_{WT}$ structure
233 by re-solving it (Figure 5, A and B, Figure S3, B and E, Table S2). S319 is part of the surface-
234 exposed loop harboring S317. In a previous study (Pinger, Nešić and Ali, et al., 2018), both by
235 crystallography and mass spectrometry, glycosylation of S319 was not clearly present (likely
236 due to intrinsic lability of the moiety). However, here we were able to observe strong density
237 for the sugar on S319 in the $VSG3_{WT}$ and $VSG3_{S317A}$ mutant crystal structures, as well as to
238 confirm the presence of hexose groups on S317 and S319 by mass spectrometry (Figure S7).
239 Subsequent determination of the crystal structures of the S319A mutant as well as the double
240 mutant (combining S317A and S319A, or "SSAA") did not reveal any significant structural
241 differences when compared to $VSG3_{WT}$ or $VSG3_{S317A}$ (Figure 5, A and B, Figure S3, B and F-
242 H).

243 Following the experimental protocol that we had used to assess the quality of the
244 repertoires elicited by $VSG3_{WT}$ and $VSG3_{S317A}$, we also generated plasma cell antibody
245 repertoires elicited by $VSG3_{S319A}$ and $VSG3_{SSAA}$, (Figure 5C) and tested those for their ability
246 to bind either their cognate parasites or to cross-react with the wild type and other mutants. We
247 found that $VSG3_{SSAA}$ parasites elicited repertoires very similar to those elicited by the
248 $VSG3_{S317A}$ mutant alone (e.g., dominant presence of the gn33 light chain V gene and 30-60.6.70

249 or J558.26.116 heavy chain gene), whereas $VSG3_{S319A}$ single mutants elicited broader
250 repertoires that were very similar to those elicited by $VSG3_{WT}$ (no gn33 dominance for
251 example) (Figure 5C). In turn, this suggests that the $VSG3_{WT}$ repertoire is strongly influenced
252 by the one-to-three hexoses linked to S317 (Pinger, Nešić and Ali, et al., 2018), but negligibly
253 by the glycans linked to S319; similarly, that the S317A determined repertoire is indifferent to
254 the presence of the sugar on S319, as the repertoire does not change in the double mutant.

255 We then tested recombinant antibodies that were elicited after infection with each of these
256 variants for the ability to cross-react with each of the other variants, we identified four classes
257 of binders:

258 (a) Antibodies that could bind all four variants (like ab239 or ab222, Figure 6, A and B);
259 these were elicited by both $VSG3_{WT}$ and $VSG3_{SSAA}$ suggesting that they bind a common
260 peptide epitope at a distance from the epitope defining sugar.

261 (b) Antibodies that bound only the epitope-defining sugar-containing variants $VSG3_{WT}$ and
262 $VSG3_{S319A}$ (like ab250, Figure 6, A and B) but not the other two variants; suggesting that they
263 bind the sugar containing epitope but not the same epitope without the carbohydrate (and are
264 therefore potentially sugar-selective);

265 (c) Antibodies that bound only the variants that lacked the epitope-defining sugar at S317
266 ($VSG3_{S317A}$ and $VSG3_{SSAA}$, like ab021); suggesting that they bind the same peptide epitope
267 defined by the sugar but are inhibited by the presence of the sugar in the other two variants.

268 (d) Finally, antibodies that only bound the $VSG3_{S317A}$ variant (e.g., ab234), potentially
269 suggestive of an additional minor epitope partly defined by the S319 sugar.

270 These results underscore the immunodominance of the relevant epitopes and the exquisite
271 discrimination of the resulting antibodies. Specifically, they suggest that the immunodominant
272 epitope that characterizes the $VSG3_{WT}$ coat is limited to the immediate amino-acids
273 surrounding the S317-*O*-glucose (including that sugar but excluding its companion on S319).

274 **Discussion**

275 The antibody-mediated interactions between host and trypanosomes have been
276 intensively studied over the years, but remain poorly understood. Investigating immune
277 responses against the coat of the trypanosomes, together with the cognate VSG structures, will
278 provide greater insights into the nature of such interactions. Here we show that mouse infection
279 with trypanosomes of a specific VSG coat leads to robust plasma cell expansion, comprised of
280 cells that are remarkably restricted in their antibody repertoire. This expansion is reminiscent
281 of acute infection with Dengue in humans (Waickman et al., 2020). It is important to note
282 however that repertoires elicited by Dengue are hypermutated and show a high degree of
283 clonality, suggesting prior exposure. In contrast, repertoires elicited by VSGs are essentially
284 unmutated (Fig. 4C and 6B). Furthermore, although each VSG gene appears to elicit a distinct
285 V gene signature, the antibodies characterized by this signature are not clonal (i.e., they contain
286 different D_H and J_H segments and consequently different CDR3 sequences). Though the
287 existence of a robust serological response to trypanosome infection has been recognized for
288 years (most recently by (Verdi and Zipkin et al., 2020), our work confirms that this response is
289 polyclonal (Müller et al., 1996). Such polyclonal (and potentially autoreactive) antibodies have
290 been documented in other infections as well, e.g., influenza (Lee et al., 2016, 2019; Woods et
291 al., 2007), dengue (Correa et al., 2015; Waickman et al., 2020), hepatitis C (de Vita et al., 2008)
292 and HIV (Moir and Fauci, 2009). Our work extends these findings by demonstrating that this
293 polyclonal response is highly stereotyped between animals, is VSG-specific and is repertoire
294 restricted.

295 The usage of distinct V gene signatures per VSG-elicited repertoire, which is highly
296 reproducible between mice, implies the existence of common paratopes. In turn, this suggests
297 that each VSG contains a small cohort of immunodominant epitopes to which the common
298 paratopes might map. To date, co-crystal structures of VSGs and cognate antibodies are not
299 available, and thus a definitive assignment of antibody-bound epitopes cannot be made.

300 However, mutations in structurally-defined features of each VSG can lead to loss of antibody
301 binding, suggesting that key immunodominant epitopes reside within a tightly circumscribed
302 region of each VSG. For VSG2, such a feature is the calcium binding pocket, identified on the
303 top lobe of the molecule: disruption of the pocket by point mutations in the calcium
304 coordinating residues (DND) did not lead to structural alteration but did result in loss of
305 recognition by $VSG2_{WT}$ -elicited antisera and monoclonal antibodies. This implies that the
306 subdomain of $VSG2_{WT}$ that contains the DND motif forms an epitope that dominates the
307 antibody response against this specific coat.

308 Similarly, for VSG3, an immunodominant epitope is defined by a small region
309 surrounding the *O*-linked glucose on serine 317. Previous work had shown that this particular
310 hexose anchors a chain of up to three additional hexoses to S317, leading Pinger et al (Pinger,
311 Nešić and Ali, et al., 2018) to hypothesize that hexose heterogeneity contributed to repertoire
312 diversification that would be detrimental to the immune response against the organism (Pinger,
313 Nešić and Ali, et al., 2018). Indeed, we found that infections with $VSG3_{S317A}$ coated
314 trypanosomes elicited restricted antibody repertoires with a V_L gene signature dominated by V_L
315 -gn33, but that this signature disappeared after infection with the wildtype VSG3 strain. This
316 loss of signature correlates with increased virulence: infection with $VSG3_{S317A}$ coated
317 trypanosomes is naturally cleared while infection with the wildtype is lethal (Pinger et al.,
318 2017). Perhaps equally interesting is the finding that a second hexose at a neighboring residue
319 to S317 (S319) plays almost no role in defining the repertoire: mutating S319 to alanine resulted
320 in a repertoire that matched the repertoire elicited by the wildtype VSG3 strain (Fig. 5C).
321 Furthermore, mutating both serines resulted in a repertoire matching that elicited by the
322 $VSG3_{S317A}$ mutant (Fig. 5C). These findings illustrate the immunodominance of key epitopes
323 on $VSG3_{WT}$, which may be limited to the amino acids in the immediate vicinity of the *O*-glycan
324 on S317, and suggest that the antibody repertoires elicited to specific VSGs not only respond

325 to defined immunodominant features within each VSG but are highly discriminatory as they do
326 so.

327 Overall, by examining two distinct VSGs and variants thereof, we demonstrate that the
328 antibody response that mediates clearance to a given *T. brucei* coat can be hyperfocused to a
329 restricted set of immunodominant epitopes that are surface exposed. Consequently, the immune
330 response elicited by each *T. brucei* variant coat has the potential to be highly restricted and
331 likely mediated by paratopes within the germline V regions of antibody genes. How *T. brucei*
332 achieves this "immunofocusing" is likely related to the highly dense, repetitive and patterned
333 nature of its surface coat. We hypothesize that this extreme focusing allows the parasite to use
334 short-tract gene conversion or even point mutations (collectively referred to as mosaic
335 formation (Hall et al., 2013; Mugnier et al., 2015) to expand its antigenicity well beyond what
336 is encoded in its considerable genomic archive. By ensuring that cross reactivity between coat-
337 defined epitopes will be exceedingly rare, even within similar variants, immunofocusing helps
338 the parasite perpetually evade the immune response.

339

340 **Acknowledgments**

341 We acknowledge synchrotron time at the Paul Scherrer Institut, Villigen, Switzerland (SLS,
342 beamline X06DA, Vincent Olieric and colleagues), the Diamond Light Source (DLS, beamline
343 i03, Neil Paterson and colleagues) and the Advanced Photon Source, Argonne National
344 Laboratory (APS, beamline 24-ID-C, Jonathan P. Schuermann and colleagues). We thank Johan
345 P. Zeelen for assistance with the synchrotron data acquisition and advice in structural
346 determination. We thank Hedda Wardemann for assistance with B cell repertoire analyses and
347 fruitful discussions especially during manuscript revision. We are grateful to Joey Verdi for
348 beneficial comments and discussion during manuscript revision. Work in the F.N.P and C.E.S
349 labs is funded by the Helmholtz Foundation. P.D.B.O and B.T.C are funded by National

Institutes of Health P41 GM109824 and P41 GM103314 to B.T.C. R.B and T.R. are supported by the German Research Foundation to T. R. (Ru 747/1-1) within in the framework of FOR 2509.

Author contributions

Conceptualization, Resources and Funding acquisition: F.N.P., C.E.S., Investigation: A.G., F.A.B., G.T., E.P.V., M.L., C.E.S., Mass Spectrometry (MS) analysis: P.D.B.O., B.T.C., R.B., T.R., ITC analysis: K.P., Formal Analysis: A.G., F.A.B., C.E.S., P.D.B.O.(MS), B.T.C.(MS), K.P.(ITC), R.B.(MS), T.R.(MS), Visualization: A.G., F.A.B., C.E.S., P.D.B.O.(MS), B.T.C.(MS), K.P.(ITC), R.B.(MS), T.R.(MS) Writing – Initial manuscript: F.N.P., C.E.S., Writing – Revised manuscript: F.N.P., C.E.S., A.G., F.A.B., G.T.

Declaration of interests

The authors declare no competing interests.

Lead Contact

Further information and requests for resources and reagents should be directed to and will be fulfilled by the lead contact, Nina Papavasiliou (n.papavasiliou@dkfz-heidelberg.de).

Data availability

Structures that support the findings of this study have been deposited in RCSB Protein Data Bank with IDs: 7P56 ($VSG2_{WT}$), 7P57 ($VSG2_{AAA}$), 7P59 ($VSG3_{WT}$), 7P5A ($VSG3_{S317A}$), 7P5B ($VSG3_{S319A}$), 7P5D ($VSG3_{SSAA}$); Mass spectrometry data are available via ProteomeXchange with identifier PXD027384; Full repertoire data are available from the corresponding authors upon reasonable request. All other data is available in the main text or the supplementary data.

Figures & Legends

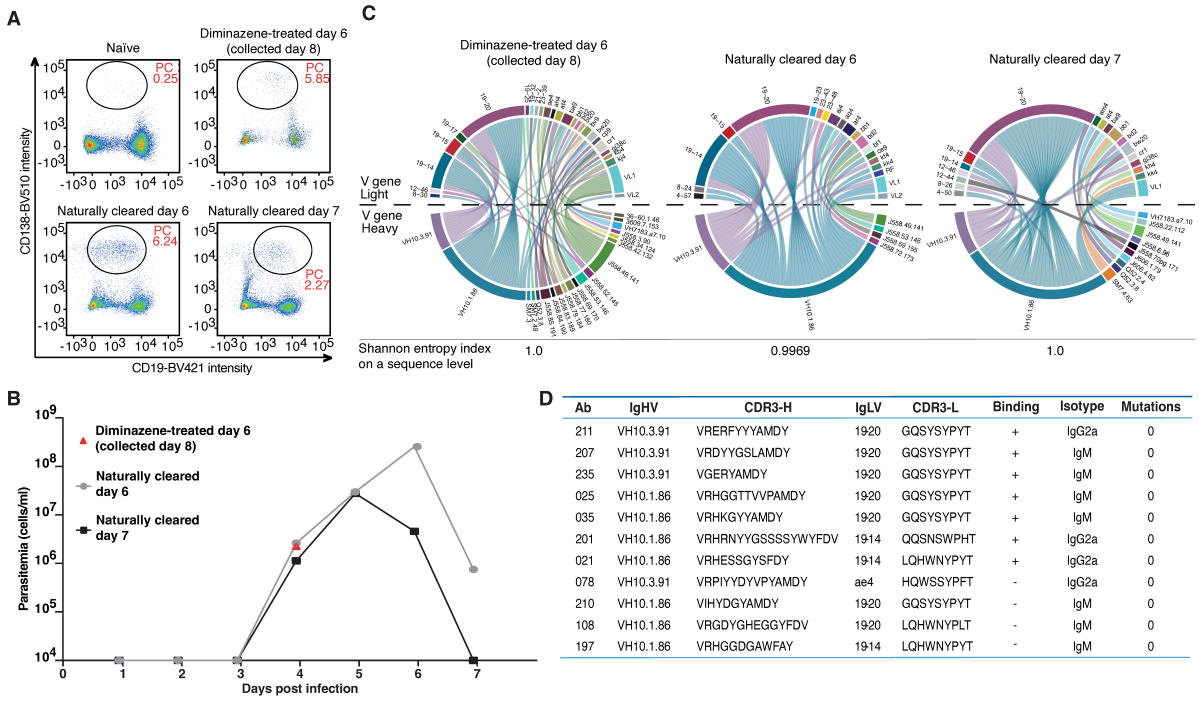

Ab	IgHV	CDR3-H	IgLV	CDR3-L	Binding	Isotype	Mutations
211	VH10.3.91	VRERFYYYAMDY	1920	GQSYSYPYT	+	IgG2a	0
207	VH10.3.91	VRDYYGSLAMDY	1920	GQSYSYPYT	+	IgM	0
235	VH10.3.91	VGERYAMDY	1920	GQSYSYPYT	+	IgM	0
025	VH10.1.86	VRHGGTTVVPAMDY	1920	GQSYSYPYT	+	IgM	0
035	VH10.1.86	VRHKGYYAMDY	1920	GQSYSYPYT	+	IgM	0
201	VH10.1.86	VRHRNYYGSSSSYWYFDV	1914	QQSNSWPHT	+	IgG2a	0
021	VH10.1.86	VRHESSGYSFDY	1914	LQHWNYPYT	+	IgG2a	0
078	VH10.3.91	VRPIYYDYVPYAMDY	ae4	HQWSSYPFT	-	IgG2a	0
210	VH10.1.86	VIHYDGYAMDY	1920	GQSYSYPYT	-	IgM	0
108	VH10.1.86	VRGDYGHEGGYFDV	1920	LQHWNYPLT	-	IgM	0
197	VH10.1.86	VRHGGDGAWFAY	1914	LQHWNYPYT	-	IgM	0

Figure 1: VSG2$_{WT}$ parasites elicit a highly restricted antibody repertoire, defined by a small number of heavy and light chain pairs. (A) Percentage of CD138+ plasma cells (PC) within the live lymphocyte population in a non-infected naïve mouse and in infected mice that were treated with diminazene or that naturally cleared the first peak of parasitemia. Plasma cells from this gate were sorted for antibody repertoire analysis. Representative gatings to determine live lymphocytes are shown in Figure S1A. **(B)** Parasitemia infection curves from the 2 mice that naturally cleared the first peak of parasitemia (panel A) at day 6 (black) and day 7 (grey). Both mice were sacrificed at day 7 post-infection. A representative value of parasitemia at day 4 for mice treated with diminazene is indicated in red. **(C)** Circos plots generated for the VSG2$_{WT}$ V gene signatures of two independent mice whose infections were treated with diminazene (left - n=89 pairs) and of two additional mice that naturally cleared the first peak of parasitemia at days 6 (center - n=53 pairs) and 7 (right - n=50 pairs) post infection. Different colors depict each heavy chain variable gene (bottom half of the plot), and each light chain variable gene (top half of the plot). The heavy and light chain variable gene pairings that form the antibodies are illustrated as connector lines starting from the heavy chain genes, providing

391 also information about the frequency of the pairings. Genes from both chains that appeared only
392 once and resulted in single heavy-light pairings, were considered background and were
393 removed from the plot. Shannon entropy shows clonal diversity on a sequence level with a
394 value of 1.0 representing 100% clonal diversity (no clones), while a value of 0.0 corresponding
395 to 0% clonal diversity (only clones). **(D)** Table with representative $VSG2_{WT}$ antibodies elicited
396 in the context of diminazene-treated infections, which are mostly composed of V*H*10 heavy
397 chains paired with 19-14 and 19-20 Vκ light chains. The CDR3 from each antibody is
398 described, indicating that the repertoire is not monoclonal. The original antibody isotype, as
399 well as somatic hypermutations, if any, are also shown.

400
401
402
403
404
405

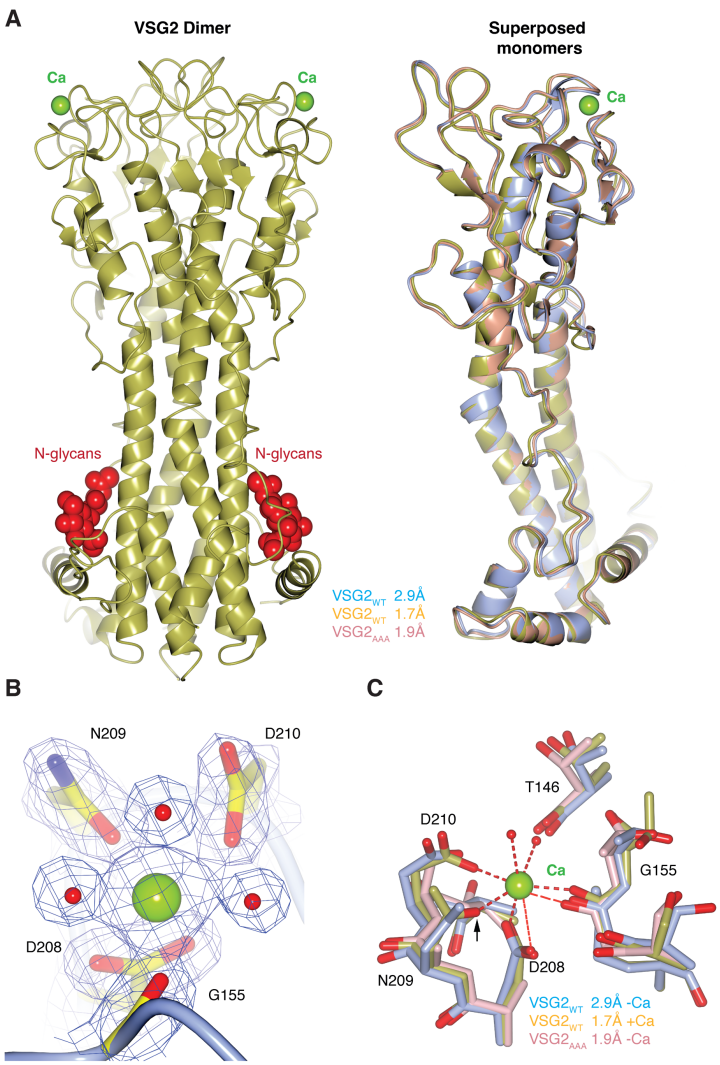

Figure 2: The resolved crystal structure of VSG2$_{WT}$ reveals the existence of a surface-exposed calcium binding pocket. **(A)** Left - Crystal structure of VSG2$_{WT}$. The homodimer is shown as a ribbon diagram colored in gold, N-linked glycans and calcium atoms are displayed as red and green space-filling atoms, respectively. Right – Structural alignment of monomers of VSG2$_{WT}$ (from left panel, in gold), VSG2$_{WT}$ (from (Freymann et al., 1990), in blue) and VSG2$_{AAA}$ (in pink), highlighting the coordination of the calcium atom. **(B)** Close-up of the coordination of calcium binding pocket with corresponding electron density maps. Water molecules and calcium atoms are displayed as red and green space-filling atoms, respectively.

415 **(C)** Superposition of the calcium binding pockets of the 3 structures presented in (A). Water
416 molecules and calcium atoms are displayed as red and green space-filling atoms, respectively.
417

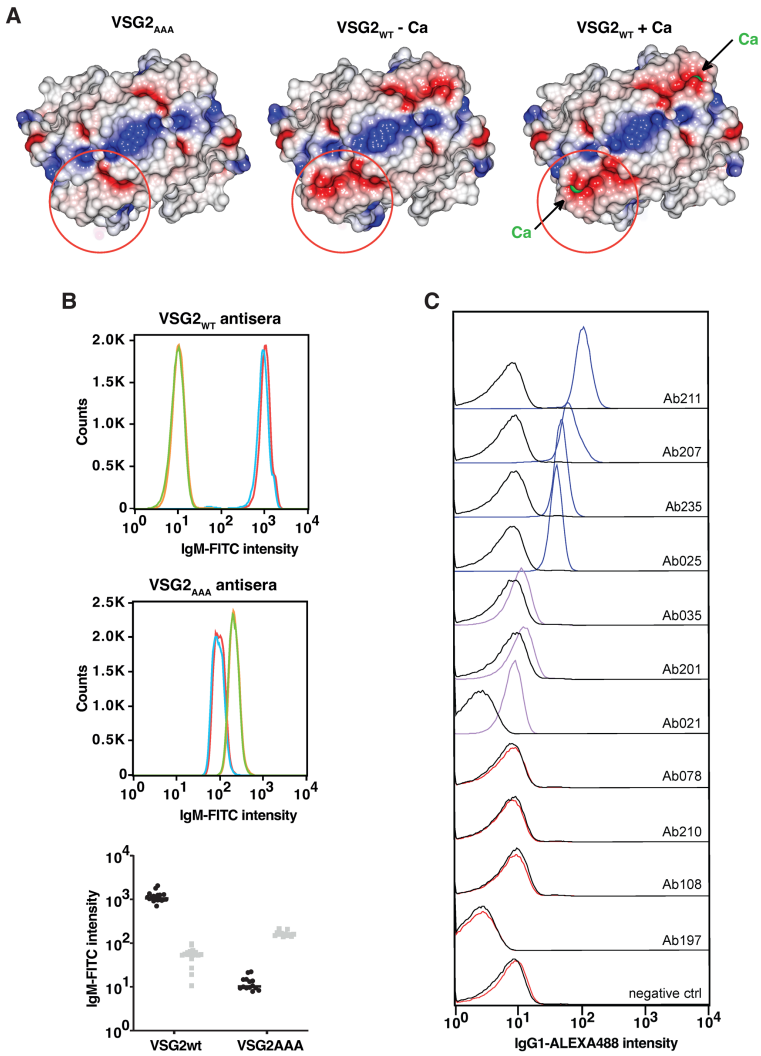

Figure 3: Residues surrounding the calcium binding pocket of VSG2$_{WT}$ define an immunodominant epitope. **(A)** Molecular surfaces of VSG2$_{WT}$ + calcium (this study), VSG2$_{WT}$ - calcium (from (Freymann et al., 1990)) and VSG2$_{AAA}$. The VSGs are oriented looking 'down' on the top lobe of the protein, the orientation rotated 90° about a horizontal axis in comparison to upper panels. The surfaces are colored by relative electrostatic potential (blue is basic/positively charged, red is acidic/negatively charged, and white is neutral). **(B)** Histograms reflecting binding intensities of antisera collected from mice infected with VSG2$_{WT}$ and VSG2$_{AAA}$ parasites (top two panels, respectively) with VSG2$_{WT}$ and VSG2$_{AAA}$ parasites (blue and red correspond to 2 independent clones of VSG2$_{WT}$ parasites; green and orange correspond to 2 independent clones of VSG2$_{AAA}$ parasites). Bottom panel shows quantification

428 of binding intensities of antisera collected from mice infected with $VSG2_{WT}$ (black dots) and
429 $VSG2_{AAA}$ (grey dots) parasites with $VSG2_{WT}$ and $VSG2_{AAA}$ parasites (median from n=12-18).
430 **(C)** Histograms reflecting binding intensities of the antibodies presented in Figure 1D with wild
431 type parasites (colors) and AAA-mutant parasites (black). Different colors are meant to
432 distinguish differential binding intensity: red – no binding; purple – poor binding; blue – good
433 binding. The gating strategy is shown in Figure S1C.

434
435

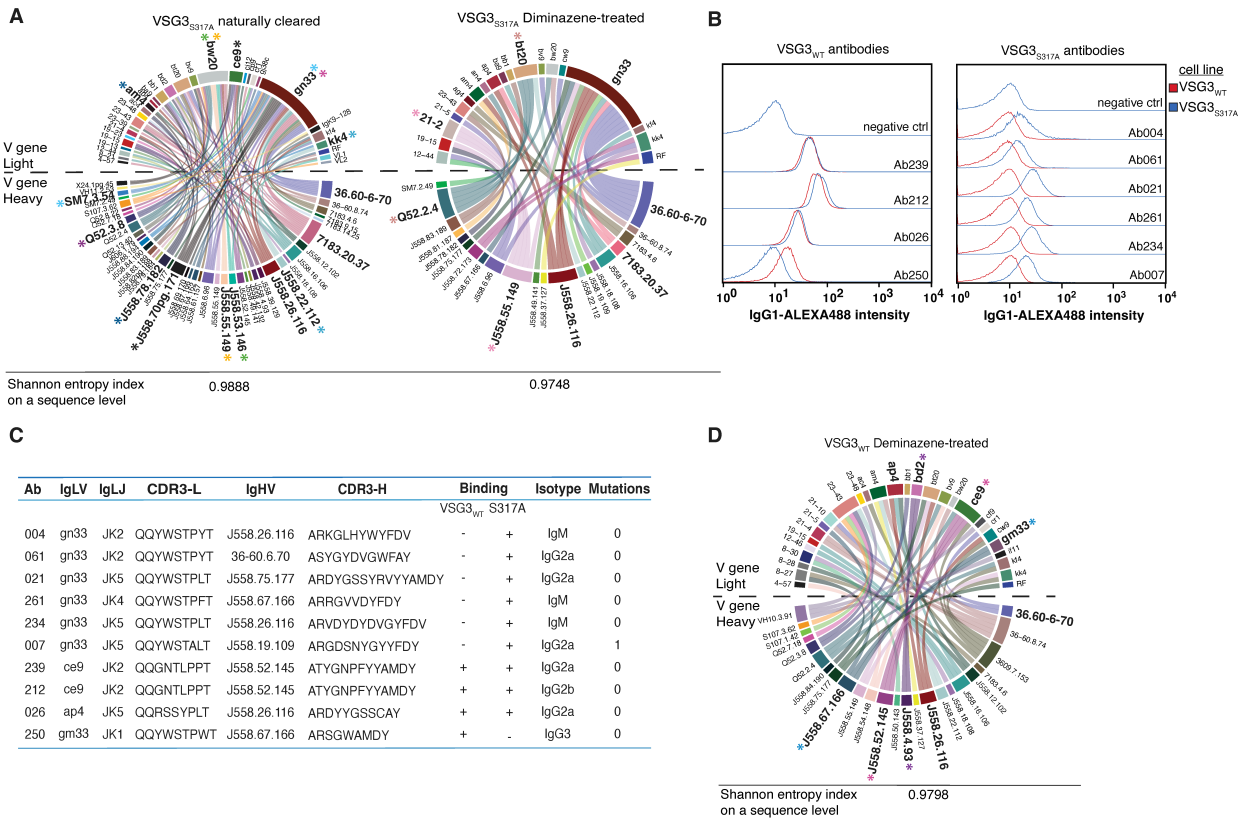

Ab	IgLV	IgLJ	CDR3-L	IgHV	CDR3-H	Binding		Isotype	Mutations
						VSG3WT	S317A		
004	gn33	JK2	QQYWSTPYT	J558.26.116	ARKGLHYWYFDV	-	+	IgM	0
061	gn33	JK2	QQYWSTPYT	36-60.6.70	ASYGYDVGWFAY	-	+	IgG2a	0
021	gn33	JK5	QQYWSTPLT	J558.75.177	ARDYGSSYRVYYAMDY	-	+	IgG2a	0
261	gn33	JK4	QQYWSTPFT	J558.67.166	ARRGVVDYFDY	-	+	IgM	0
234	gn33	JK5	QQYWSTPLT	J558.26.116	ARVDYDYDVGYFDV	-	+	IgM	0
007	gn33	JK5	QQYWSTALT	J558.19.109	ARGDSNYGYYFDY	-	+	IgG2a	1
239	ce9	JK2	QQGNTLPPT	J558.52.145	ATYGNPFYYAMDY	+	+	IgG2a	0
212	ce9	JK2	QQGNTLPPT	J558.52.145	ATYGNPFYYAMDY	+	+	IgG2b	0
026	ap4	JK5	QQRSSYPLT	J558.26.116	ARDYYGSSCAY	+	+	IgG2a	0
250	gm33	JK1	QQYWSTPWT	J558.67.166	ARSGWAMDY	+	-	IgG3	0

Figure 4: VSG3$_{S317A}$ parasites elicit a restricted B cell response, with preferential utilization of a light chain Vκ gene (gn33). (A) Circos diagrams generated for the VSG3$_{S317A}$ V gene signatures of four mice infections, two naturally cleared (left - n=114 pairs) and two diminazene treated (right - n=48 pairs). Different colors depict each heavy chain variable gene (bottom half of the plot), and each light chain variable gene (top half of the plot). The heavy and light chain variable gene pairings that form the antibodies are illustrated as connector lines starting from the heavy chain genes, providing also information about the frequency of the pairings. Genes from both chains that appeared only once and resulted in single heavy-light pairings, were considered background and were removed from the plot. Colored-asterisks depict individual B cells that correspond to clones (i.e., share the same V heavy and V light gene segments but also the same DJ or J genes and the same CDR3 length and sequence). Shannon entropy shows clonal diversity on a sequence level, a number of 1.0 shows 100% clonal diversity (no clones), while a value of 0.0 corresponds to 0% clonal diversity (only clones). **(B)** Left: FACS analysis of heavy and light chain pairs selected from the VSG3$_{WT}$

450 repertoire, produced recombinantly as IgG1 antibodies. The plots depict antibody binding to
451 $VSG3_{WT}$ (red) or $VSG3_{S317A}$ (blue) *T. brucei* cells. Parasites were first stained with each
452 antibody supernatant, and counter stained with (mouse anti-human) AlexaFluor488-IgG1
453 secondary antibody. The gating strategy is shown in Figure S1C. Staining with supernatants
454 from untransfected cells (no plasmid) serves as a negative control. All data are normalized to
455 mode. Right: FACS showing the same experimental setup but now for binding of recombinant
456 antibodies selected from the $VSG3_{S317A}$ repertoire. **(C)** Table of all the $VSG3_{S317A}$ antibodies
457 with gn33 as a light chain that bound to the cognate and WT cells, as well as of all the $VSG3_{WT}$
458 antibodies and their binding to cognate and mutant cells. The (+) symbol indicates binding
459 while the (-) lack of binding. V and J segments as well as the CDR3 of both heavy and light
460 chain genes are shown, along with the binding to the respective parasites. The original antibody
461 isotype, as well as somatic hypermutations, if any, are also shown**. (D)** Circos plots generated
462 for the $VSG3_{WT}$ V gene signatures from two mice whose infections were treated with
463 diminazene (n=53 pairs), as described in (A).
464

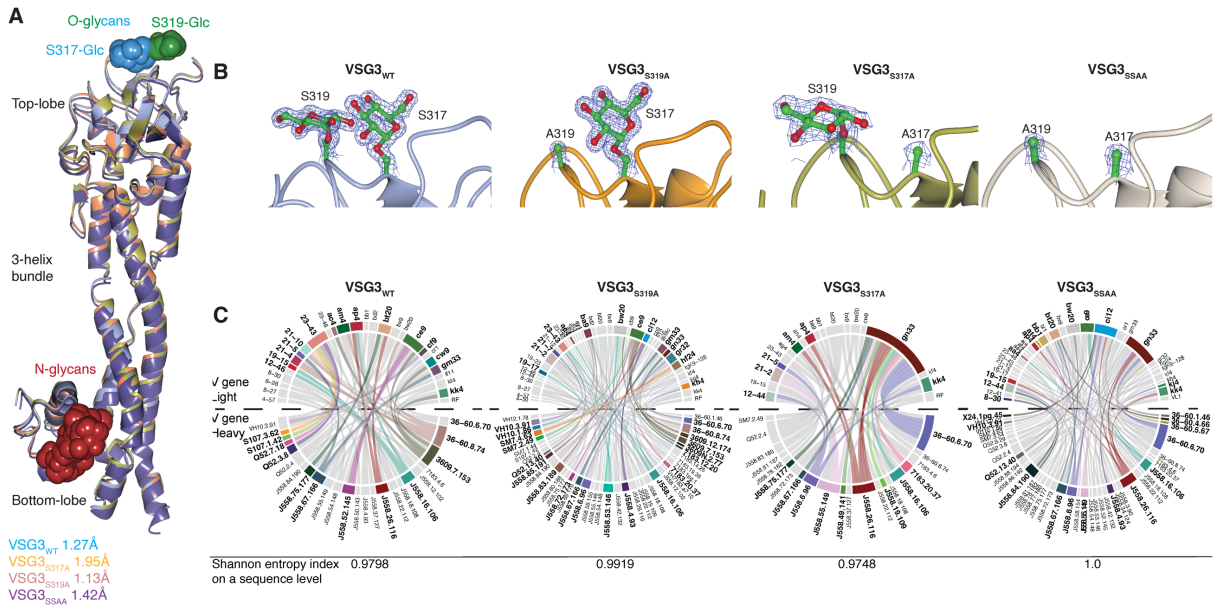

Figure 5: Nearly identical VSG3 variant coats elicit distinct V gene signatures. **(A)** Overlaid crystal structures of all four VSG3 monomers, shown as ribbon diagrams and colored in blue (WT), gold (S317A), salmon (S319A) and purple (SSAA). The N-glycans are represented as red spheres on the bottom lobe, while the *O*-linked sugars as blue (S317-sugar) and green (S319-sugar) spheres on the top lobe. **(B)** Electron density maps maps (2Fo-Fc, contoured at 1σ) focused on the presence or absence of the S317 and S319 *O*-Glucose molecules for all individual proteins as indicated in the labeling. **(C)** Circos plots of the diminazene-treated plasma cell antibody repertoires (V signatures shown only) of WT (n=53 pairs), S317A (n=48 pairs), S319A (n=109 pairs) and SSAA (n=102 pairs). Different colors depict each heavy chain variable gene (bottom half of the plot), and each light chain variable gene (top half of the plot). The heavy and light chain variable gene pairings that form the antibodies are illustrated as connector lines starting from the heavy chain genes, providing also information about the frequency of the pairings. Genes from both chains that appeared only once and resulted in single heavy-light pairings, were considered background and were removed from the plot. The antibody pairs picked for validation are presented in color, while all other genes are in gray.

Shannon entropy shows clonal diversity on a sequence level (a value of 1.0 shows 100% clonal diversity (no clones), while a value of 0.0 corresponds to 0% clonal diversity (only clones)).

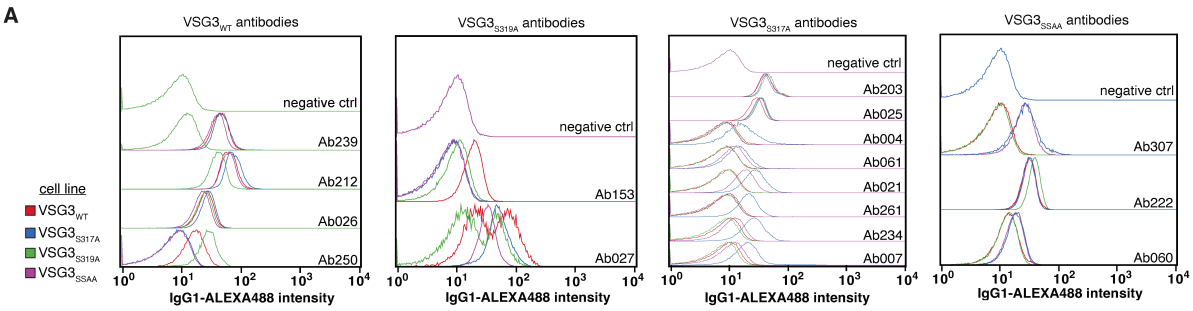

B

Ab	IgLV	IgLJ	CDR3-L	IgHV	CDR3-H	Binding				Isotype	Mutations
						$VSG3_{WT}$	S317A	S319A	SSAA		
234	gn33	JK5	QQYWSTPLT	J558.26.116	ARVDYDYDVGYFDV	-	+	-	-	IgM	0
021	gn33	JK5	QQYWSTPLT	J558.75.177	ARDYGSSYRVYYAMDY	-	+	-	+	IgG2a	0
250	gm33	JK1	QQYWSTPWT	J558.67.166	ARSGWAMDY	+	-	+	-	IgG3	0
222	aa4	JK2	QQYHSYPPT	J558.16.106	ARLFYYGSSPYFDY	+	+	+	+	IgM	0
239	ce9	JK2	QQGNTLPPT	J558.52.145	ATYGNPFYYAMDY	+	+	+	+	IgG2a	0

Figure 6: Antibodies elicited by VSG3 variants fall into four classes based on their antigen binding capacity. **(A)** FACS data showing the binding of the validated antibodies, secreted as IgG1s, to $VSG3_{WT}$ (red), $VSG3_{S317A}$ (blue), $VSG3_{S319A}$ (green) and $VSG3_{SSAA}$ (purple) - covered trypanosomes. Parasites were first stained with each antibody supernatant, followed by staining with a (mouse anti-human) AlexaFluor488-IgG1 secondary antibody. The gating strategy is shown in Figure S1C. Staining with supernatants from untransfected cells (no plasmid) is used as a negative control. All data were normalized to mode. **(B)** Table of representative binding patterns of the produced antibodies (also in 4, B and C) to different trypanosome cell lines. The (+) symbol indicates binding while the (-) non-binding. V and J segments as well as the CDR3 of both heavy and light are shown, along with the binding to the individual cell lines. The original isotypes and somatic hypermutations, if any, are also listed.

500 **Star Methods**

501 **Trypanosome cell lines and mouse strains.**

502 All trypanosome cell lines used in this study were bloodstream-form trypanosomes
503 derived from the Lister-427 "2T1" cell line (Alsford et al., 2005) and were cultivated *in vitro*
504 in HMI-9 medium (Hirumi and Hirumi, 1989) (formulated as described by PAN Biotech
505 without FBS, l-cysteine or β-mercaptoethanol), supplemented with 10% fetal calf serum
506 (Gibco), l-cysteine and β-mercaptoethanol. Cells were cultured at 37 °C and 5% CO2. The
507 $VSG3_{WT}$ and $VSG3_{S317A}$ cell lines were described before (Pinger, Nešić and Ali, et al., 2018).
508 Isogenic $VSG3_{S319A}$ and $VSG3_{SSAA}$ mutant clones were derived from transfection of 2T1
509 (VSG2 expressing) cells with the pAG plasmids described below, and then initially selected
510 based on loss of VSG2 expression and gain of VSG3 expression (by FACS, see below).
511 Derivation of isogenic $VSG2_{WT}$ or $VSG2_{AAA}$ mutant trypanosomes was achieved through
512 transfection of naturally occurring switchers of 2T1 (expressing VSG3, or VSG9) with the
513 relevant pFAB plasmids (see below), and then initially selected based on gain of VSG2
514 expression.

515 These strains were used to infect female, wild-type C57BL/6J mice, aged 6–8 weeks at
516 experiment start (Janvier). Mice were kept in IVC cages under SPF conditions in the animal
517 facility at the German Cancer Research Center (DKFZ, Heidelberg). All animal experiments
518 were performed in accordance with institutional and governmental regulations, and were
519 approved by the Regierungspräsidium (Karlsruhe, Germany).

520

521 **Engineering plasmids used to generate isogenic *T. brucei* clones expressing VSG2 or VSG3**
522 **and mutants thereof.**

523 Plasmids used to generate $VSG3_{WT}$ and $VSG3_{S317A}$ -expressing cells were described in
524 (Pinger, Nešić and Ali, et al., 2018). Modifications of these plasmids using site-directed

525 mutagenesis (Q5, New England Biolabs) were used to generate $VSG3_{S319A}$ (pAG1) and the
526 $VSG3_{SSAA}$ -expressing cells (pAG2). Plasmids were first linearized by EcoRV (New England
527 Biolabs), and then transfected into VSG2-expressing cells (2T1).

528 Plasmids used to generate VSG2 and $VSG2_{AAA}$ isogenic strains (pFAB1 and pFAB4
529 respectively) were created using vector pSY371D-CTR-BSD (Pinger et al., 2017) as a
530 backbone (also modified to contain the hygromycin-resistance gene (HYG) instead of
531 blasticidin). pFAB1 and pFAB4 were linearized with BglII (New England Biolabs) prior to
532 transfection.

533

534 ***T. brucei* transfections, clone selection and verification.**

535 All transfections were performed using 10ug of each plasmid mixed with 100ul of 2.5-
536 $3x10^7$ cells in homemade Tb-BSF buffer (90mM Na_2HPO_4, pH 7.3, 5mM KCl, 0.15mM $CaCl_2$,
537 50mM HEPES, pH7.3), using the AMAXA nucleofector (Lonza) program X-001, as previously
538 described (Burkard et al., 2007). After 6h, blasticidin at a concentration of 100ug/ml
539 ($VSG3_{S319A}$ and $VSG3_{SSAA}$ cell lines) or hygromycin at 25ug/ml ($VSG2_{WT}$ and $VSG2_{AAA}$ cell
540 lines) were added and single-cell clones were obtained by serial dilutions in 24-well plates and
541 harvested after 5 days. The $VSG3_{S319A}$ and $VSG3_{SSAA}$ clones were screened by FACS for VSG3
542 expression and VSG2 loss of expression and $VSG2_{WT}$ and $VSG2_{AAA}$ clones for VSG2
543 expression using monoclonal antibodies against these VSGs (Pinger et al., 2017). Positive
544 clones were sequenced by isolating RNA using the RNeasy Mini Kit (Qiagen), followed by
545 DNAse treatment with the TURBO DNA-free kit (Invitrogen) and cDNA synthesis with
546 ProtoScript II First Strand cDNA Synthesis (New England Biolabs). The sequences were then
547 amplified, using Phusion High-Fidelity DNA Polymerase (New England Biolabs), a forward
548 primer binding to the spliced leader sequence and a reverse binding to the VSG 3´untranslated

549 region. The final products were purified by gel extraction from a 1% gel with the NucleoSpin
550 Gel and PCR clean-up kit (Macherey-Nagel) and sent for Sanger sequencing.
551
552 **Spleen and antisera collection**.
553 6-8-week-old C57BL/6J wild-type mice were injected intraperitoneal (i.p.) with
554 1×10^3 parasites in HMI-9. Mice that cleared $VSG3_{S317A}$ infections naturally, were injected i.p.
555 with 100 parasites in HMI-9. Mice treated with diminazene underwent an injection (i.p.) of
556 250 ng diminazene aceturate (Abcam)/mouse 4 days after infection, and this procedure was
557 repeated after 24 h. On day 8 post parasite injection, mice were euthanized with CO2. Mice that
558 naturally cleared the first peak of parasitemia were carefully monitored three times per day
559 between days 5-7 post infection and euthanized with CO2 upon clearance of parasitemia.
560 After mice were euthanized, blood was collected via cardiac puncture and serum was
561 separated from whole blood using Microtainer SST serum collection tubes (BD 365968).
562 Spleen was also collected and single-cell suspensions were prepared by standard procedures.
563
564 **Flow Cytometry and Single Cell Sorting.**
565 Splenocytes from spleens of Trypanosome-infected mice were thawed, washed in RPMI
566 media (Gibco) at room temperature, centrifuged at 2000 rpm for 5 min and resuspended in
567 100ul 2% FBS/PBS. Cells were stained with rat anti-mouse CD19-BV421 (1:100, Biolegend),
568 rat anti-mouse CD138-BV510 (1:300, Biolegend), rat anti-mouse IgG1-BV650 (1:100,
569 Biolegend) and goat anti-mouse IgM-Biotin (1:400, Jackson Laboratories) for 45 min on ice in
570 the dark. Biotin was detected using Streptavidin-BV785 (1:400, Biolegend) and 7-
571 Aminoactinomycin D (7AAD) (1:200, Invitrogen) was used as a dead cell marker in all
572 samples. The cells were analyzed on a LSRFortessa instrument (BD Bioscience), single-cell
573 sorted into 384-well plates (black frame, 4titude) using either an Aria I or Aria Fusion II cell

574 sorter (BD Bioscience) and analyzed using FlowJo software (v10). For single-cell sorting, the
575 plasma cell population was defined as $7AA^{-}CD19^{lo}CD138^{+}$ and was checked for IgM and IgG1
576 surface expression, without including these markers in the gating of the sort population. The
577 exact isotype of each plasma cell was determined later by sequence analysis.

578

579 **Antibody repertoires, cloning and production of mouse antibodies.**

580 Ig heavy (IgH), kappa (Igκ) and lambda (Igλ) genes from single plasma cells were
581 amplified as described before (Tiller et al., 2008). Briefly, cDNA of each cell was produced
582 using random hexameric primers and then the IgH, Igκ and Igλ gene transcripts were amplified
583 by a subsequent semi-nested PCR approach using V segment and constant region-specific
584 primers (Tiller et al., 2008). The PCR products were sent for Sanger sequencing and analyzed
585 with the IgBlast online tool (NCBI, (Ye et al., 2013)) to generate the antibody repertoires.
586 Matching heavy and light pairs originating from the same cell were picked, amplified using V
587 and J gene-specific primers that include restriction sites for cloning and cloned into appropriate
588 human expressing vectors (Tiller et al., 2008). After they were successfully cloned and their
589 sequence was validated, the corresponding heavy and light chain plasmids were co-transfected
590 into adherent HEK293T cells (ATCC) using Lipofectamine 2000 (Invitrogen) reagent in 1x
591 OptiMEM (Gibco). After 6h the media was removed and cells were supplemented with 1x
592 Nutridoma-SP (Roche). Supernatants containing the produced antibodies (as IgG1) were
593 collected after 48h and 96h and tested for their ability to bind to live trypanosomes by FACS.

594

595 **VSG purification.**

596 VSGs were purified as described in (Cross, 1984) with minor changes. Briefly, cells
597 grown to a density of $2.5\text{-}4 \times 10^{6}$ were centrifuged and lysed in 0.2mM $ZnCl_2$. Following cell
598 lysis, the mixture was centrifuged and the pellet containing the VSG protein was resuspended

599 in prewarmed (40ºC) 20mM HEPES buffer, pH 8.0, supplemented with 150mM sodium
600 chloride ($VSG2_{WT}$ and $VSG2_{AAA}$) or 20mM HEPES buffer, pH 7.5, supplemented with 150mM
601 sodium chloride ($VSG3_{WT}$ and the three sugar-mutants). After a second centrifugation, the
602 supernatants containing the VSG protein were loaded onto an anion-exchange column (Q
603 Sepharose Fast Flow, GE Healthcare) previously equilibrated with the respective HEPES buffer
604 as above. The flow-through and two washes containing the VSG of interest were collected and
605 concentrated using an Amicon Stirred Cell (Merck Millipore) and the sample was then run over
606 a gel filtration column (Superdex 200, GE Healthcare) after equilibration with the respective
607 HEPES buffer as above. Aliquots of both the different purification steps and the gel filtration
608 runs were subjected to SDS-PAGE analysis for visual inspection (Figure S3, C-H). From the
609 gel filtration step onwards, all VSG3 constructs were gradually carboxy-terminal (CTD)
610 truncated, likely due to cleavage by endogenous proteases, resulting in the crystallization of
611 only the N-terminal domain. For crystallization of $VSG2_{AAA}$, VSG purified from gel filtration
612 was concentrated to 2.2mg/ml and left for 1 week at 4ºC where the CTD was also truncated
613 (again, likely due to endogenous proteases). $VSG2_{AAA}$ underwent a second gel filtration
614 (Superdex 200, GE Healthcare) and was concentrated to 4.8mg/ml. For crystallization of
615 $VSG2_{WT}$, VSG was first purified with the same protocol but using 20mM Tris, pH 8.0. After
616 passage over an anion-exchange column, VSG was concentrated to 10mg/ml and passed over
617 a gel filtration column (Superdex 200, GE Healthcare) equilibrated in 20 mM Tris pH 8.0.
618 Aliquots from the gel filtration runs were subjected to SDS–PAGE analysis for visual
619 inspection, and concentrated to 2.5mg/ml.

620

621 **Crystallization and structural determination.**

622 Native crystals of $VSG2_{WT}$ were grown by vapor diffusion using hanging drops formed
623 from mixing a 1:1 volume ratio of the protein with an equilibration buffer consisting of 0.1M
624 K-acetate, 22% PEG8000. For cryoprotection, crystals were transferred directly into a buffer

625 with a 25% PEG 8000, 0.1M K-acetate, 20% glycerol and flash-cooled immediately afterward
626 to 100 K (−173.15 °C). Data were collected at Advanced Photon Source (APS) at Argonne
627 National Laboratory at beamline 24-ID-C and processed onsite through the RAPD software
628 pipeline. The structure was solved by molecular replacement using the model of PDB entry
629 1VSG with the PHENIX software suite (Adams et al., 2010). The model was improved and
630 finalized through several cycles of auto-building (PHENIX), manual adjustment, and
631 refinement (PHENIX) (Table S1).

632 Native crystals of $VSG2_{AAA}$ were grown by vapor diffusion using hanging drops formed
633 from mixing a 1:1 volume ratio of the protein with an equilibration buffer consisting of 0.1M
634 Tris pH 8.0, 39% PEG400. This equilibration buffer is cryoprotective and crystals were flash-
635 cooled afterward to 100 K (−173.15 °C). Data were collected at the Swiss Light Source (SLS)
636 at a wavelength of 1.0Å on beamline X06DA (PXIII) The structure was solved by molecular
637 replacement using the model of PDB entry 1VSG with the PHENIX suite (Adams et al., 2010).
638 The model was improved and finalized through several cycles of auto-building (PHENIX),
639 manual adjustment, and refinement (PHENIX) (Table S1).

640 Purified $VSG3_{WT}$ and the three sugar-mutants were concentrated to 2mg/ml in 20mM
641 HEPES buffer, pH 7.5, supplemented with 150mM NaCl. Crystals were grown at 22ºC by vapor
642 diffusion using hanging drops with a 1:1 volume ratio of protein to equilibration buffer
643 consisting of 21% PEG 3350, 250mM NaCl and 100mM Tris, pH 8.2 for $VSG3_{WT}$ and
644 $VSG3_{S317A}$ and 25% PEG 3350, 300mM NaCl and 100mM HEPES, pH 7.5 for $VSG3_{S319A}$ and
645 $VSG3_{SSAA}$. For cryoprotection the crystals were transferred to the same buffer as that used for
646 equilibration but supplemented with 25% v/v glycerol and were flash-frozen in liquid nitrogen.
647 Data for $VSG3_{WT}$, $VSG3_{S317A}$ and $VSG3_{SSAA}$ were collected at the Swiss Light Source (SLS)
648 at a wavelength of 1.0Å on beamline X06DA (PXIII) and for $VSG3_{S319A}$ at the Diamond Light
649 Source at a wavelength of 0.9763Å on beamline i03. The $VSG3_{WT}$ and sugar-mutant structures
650 were obtained using the previously solved $VSG3_{WT}$ structure (PDB ID: 6ELC) (Pinger, Nešić

651 and Ali, et al., 2018) as a model to perform Molecular Replacement in the PHENIX suite
652 (Adams et al., 2010). The models were improved and finalized through several cycles of auto-
653 building (PHENIX), manual adjustment, and refinement (PHENIX) (Table S2).
654
655 **Mass Spectrometry.**
656 Purified $VSG2_{WT}$ and $VSG2_{AAA}$ samples were buffer-exchanged into native Mass
657 Spectrometry (nMS) solution (150mM ammonium acetate, 0.01% Tween-20, pH7.5) using
658 Zeba desalting microspin columns with a 40-kDa molecular weight cut-off (Thermo Scientific).
659 An aliquot (2–3µL) of the buffer-exchanged sample was loaded into a gold-coated quartz
660 capillary tip that was prepared in-house. The sample was then electrosprayed into an Exactive
661 Plus EMR instrument (Thermo Fisher Scientific) using a modified static nanospray source
662 (Olinares and Chait, 2020). The MS parameters used included: spray voltage, 1.1 – 1.3kV;
663 capillary temperature, 200°C; S-lens RF level, 200; resolving power, 35,000 at *m/z* of 200;
664 AGC target, 1 – 3 x 10^6; number of microscans, 5; maximum injection time, 200ms; in-source
665 dissociation (ISD), 200V; injection flatapole, 8V; interflatapole, 7V; bent flatapole, 6V; high
666 energy collision dissociation (HCD), 10V; ultrahigh vacuum pressure, 5×10^{-10} mbar; total
667 number of scans, 100. Mass calibration in positive mode was performed using cesium iodide.
668 Raw nMS spectra were visualized using Thermo Xcalibur Qual Browser (version 4.2.47).
669 Deconvolution was performed using UniDec version 4.2 (Marty et al., 2015; Reid et al., 2019).
670 The UniDec parameters used were m/z range: 3,500 – 5,500; mass range: 90,000 – 105,000Da;
671 sample mass every 0.2Da; smooth charge state distribution, on; peak shape function, Gaussian;
672 and Beta softmax function setting, 20.
673 Native MS analyses of the purified VSG2 samples revealed massive heterogeneity due
674 to extensive glycosylation consistent with previous studies that determined N-glycosylation at
675 two Asn sites and variable galactosylation at the C-terminal GPI anchor per VSG2 monomer

676 (Manthri et al., 2008; Mehlert et al., 1998; Zamze et al., 1991). To reduce sample complexity
677 and enable unambiguous identification of bound metal ions, the VSG samples were N-
678 deglycosylated using PNGaseF (NEB) with and without 10mM EDTA at 37°C for 3 - 4h. The
679 deglycosylated samples were then buffer exchanged and analyzed by nMS as described above.

680 The expected masses for the VSG2 glycoforms were determined as follows. The signal
681 peptide at the N-terminus (residues 1-27) and the GPI attachment signal peptide at the C-
682 terminus (residues 460-476) were removed from the precursor $VSG2_{WT}$ sequence yielding a
683 monomer mass 46,291.8Da for the processed protein. Common to all the monomers is the
684 presence of four disulfide bridges (-8.06 Da) as well as attachment of glucosamine-α1-6-myo-
685 inositol-1,2-cyclic phosphate (+385.26 Da), ethanolamine phosphate (+123.05 Da) and five
686 hexoses (+810.70 Da) at the C-terminal GPI anchor. Moreover, PNGaseF cleavage of N-linked
687 glycans at two Asn residues results in deamidation of Asn to Asp (+1.97 Da). Overall, the
688 resulting monomer and dimer masses are 47,604.7 Da and 95,209.4 Da, respectively. Each
689 additional galactose attachment from variable galactosylation at the GPI anchor adds 162.14
690 Da. Each Ca^{2+} ion bound adds 38.06 Da (average mass of Ca minus the mass of $2H^{+}$ from
691 deprotonation of two aspartic acids that coordinate with the cation). The DND-to-AAA
692 mutation results in a decrease of $VSG2_{WT}$ dimer mass by 262.10 Da (Table S3).

693 Purified $VSG3_{WT}$ was either concentrated to 3mg/mL in 20mM HEPES, pH 8.0, with
694 150mM NaCl and sent for Electron transfer dissociation (ETD) analysis or 50ug of protein in
695 the same buffer were treated as described in (Pinger, Nešić and Ali, et al., 2018) and then
696 separated by SDS PAGE. The 17 kDa fragment was excised and processed as described
697 (Fecher-Trost et al., 2013). In brief, trypsin digestion was done overnight at 37°C. The reaction
698 was quenched by addition of 20µL of 0.1% trifluoroacetic acid (TFA; Biosolve, Valkenswaard,
699 The Netherlands) and the supernatant was dried in a vacuum concentrator before LC-MS
700 analysis. Nanoflow $LC\text{-}MS^2$ analysis was performed with an Ultimate 3000 liquid
701 chromatography system coupled to an Orbitrap Elite mass spectrometer equipped with ETD

702 (Thermo-Fischer, Bremen, Germany). Samples were dissolved in 0.1% TFA, injected to a self-
703 packed analytical column (75um x 200mm; ReproSil Pur 120 C18-AQ; Dr Maisch GmbH) and
704 eluted with a flow rate of 300 nl / min in an acetonitrile-gradient (3% - 40%). The mass
705 spectrometer was operated in data-dependent acquisition mode, automatically switching
706 between MS and MS^2. Collision induced dissociation MS^2 spectra were generated for up to 10
707 precursors with normalized collision energy of 29%. Electron transfer dissociation (ETD) MS^2
708 spectra were generated for up to 5 precursors using the default settings of the instrument. Each
709 analysis was done in triplicate.

710 Raw files were processed using Proteome discoverer 2.2 (Thermo Scientific) for peptide
711 identification and quantification. MS^2 spectra were searched against the Uniprot Trypanosoma
712 database (UniprotKB), a custom database entry with the VSG3 sequence and the contaminants
713 database (MaxQuant database; MPI Martinsried) with the following parameters: Acetyl
714 (Protein N-term), Oxidation (M) and Hex (S,T) as variable modifications and carbamidomethyl
715 (C) as static modification. Trypsin/P was set as the proteolytic enzyme with up to 2 missed
716 cleavages allowed. The maximum false discovery rate for proteins and peptides was 0.01 and
717 a minimum peptide length of 7 amino acids was required.

718

719 **Isothermal Titration Calorimetry.**

720 To evaluate binding of ions to $VSG2_{WT}$ or $VSG2_{AAA}$ and remove contaminating
721 calcium, all glassware was first treated with phosphoric acid and water to prepare all buffers
722 and solutions for treatment with Chelex 100 Resin 200-400 mesh (BioRad). Upon purification
723 of VSG2, the CTD was removed by digestion with Endoproteinase LysC (New England
724 Biolabs) at a 1:500 LysC/substrate ratio by mass together with 10mM EDTA for 5h at 37°C.
725 The samples were then run over a gel filtration column (Superdex 200, GE Healthcare) after
726 equilibration with the respective 20mM Tris pH 8.0 buffer. Afterwards, proteins were

727 concentrated to 30mM by concentration in 10-kDa disposable ultrafiltration centrifugal
728 devices.

729 ITC experiments were performed using a PEAQ ITC (Malvern) at 20°C with a
730 stirring rate of 750 rpm. Titration buffers contained 20mM Tris pH 8. In each experiment, the
731 protein concentration in the cell was 30µM. $CaCl_2$, KCl and $MgCl_2$ were injected at 600µM
732 with injection sizes of 12×3µl. The data were baseline-corrected, integrated and analysed with
733 the PEAQ ITC Analysis software (Malvern), fitted using a single-site binding model.

734

735 **Fluorescence-activated cell sorting (FACS).**

736 To assess binding of antisera to live trypanosomes, 1 x 10^6 parasites were harvested and
737 incubated with $VSG2_{WT}$ anti-sera (1:4000) or $VSG2_{AAA}$ (1:2000) together with Fc block (1:200,
738 BD Pharmingen) in cold Trypanosome Dilution Buffer (TDB) (5mM KCl, 80mM NaCl, 1mM
739 $MgSO_4$, 20mM Na_2HPO_4, 2mM NaH_2PO_4, 20mM glucose, pH 7.4) for 10 min at 4°C. Cells
740 were washed once with cold TDB and resuspended in 200µl cold TDB with rat anti-mouse
741 IgM-FITC (1:500, Biolegend). Upon one wash with cold TDB, cells were resuspended in 250µl
742 TDB and immediately analyzed with FACSCalibur (BD Bioscences) and FlowJo software
743 (v10).

744 To verify whether the repertoire antibodies that were produced in HEK cells were able
745 to bind to live trypanosomes, 0.5 x 10^6 parasites were harvested, washed once with cold HMI-
746 9 without FBS and stained in 200ul of each antibody supernatant for 10 min at 4°C. Cells were
747 pelleted, resuspended in 100ul cold HMI-9 without FBS with mouse anti-human IgG1-
748 AlexFluor488 (1:500, Invitrogen) for 10 min at 4°C in the dark. Cells were washed once with
749 cold HMI-9 without FBS, resuspended in 100ul of the same buffer and immediately analyzed
750 with FACSCalibur (BD Bioscences) and FlowJo software (v10).

751

752 **Supplementary Information**

753 Figures S1-S7

754 Tables S1-S3

755

756

757

758 **References**

759 Adams, P.D., Afonine, P. v., Bunkóczi, G., Chen, V.B., Davis, I.W., Echols, N., Headd, J.J.,
760 Hung, L.W., Kapral, G.J., Grosse-Kunstleve, R.W., et al. (2010). PHENIX: A comprehensive
761 Python-based system for macromolecular structure solution. Acta Crystallographica Section D:
762 Biological Crystallography *66*, 213–221. 10.1107/S0907444909052925

763 Alsford, S., Kawahara, T., Glover, L., and Horn, D. (2005). Tagging a T. brucei RRNA locus
764 improves stable transfection efficiency and circumvents inducible expression position effects.
765 Molecular and Biochemical Parasitology *144*, 142–148. 10.1016/j.molbiopara.2005.08.009

766 Aresta-Branco, F., Erben, E., Papavasiliou, F.N., and Stebbins, C.E. (2019). Mechanistic
767 Similarities between Antigenic Variation and Antibody Diversification during Trypanosoma
768 brucei Infection. Trends in Parasitology *35*, 302–315. 10.1016/j.pt.2019.01.011

769 Bangs, J.D. (2018). Evolution of Antigenic Variation in African Trypanosomes: Variant
770 Surface Glycoprotein Expression, Structure, and Function. BioEssays *40*.
771 10.1002/bies.201800181

772 Black, S.J., Sendashonga, C.N., O'brien, C., Borowy, N.K., Naessens, M., Webster, P., and
773 Murray, M. (1985). Regulation of Parasitaemia in Mice Infected with Trypanosoma brucei. In
774 Hudson L., eds. The Biology of Trypanosomes. Current Topics in Microbiology and
775 Immunology (Springer), pp. 93–118. 10.1007/978-3-642-70538-0_5

776 Burkard, G., Fragoso, C.M., and Roditi, I. (2007). Highly efficient stable transformation of
777 bloodstream forms of Trypanosoma brucei. Molecular and Biochemical Parasitology *153*, 220–
778 223. 10.1016/j.molbiopara.2007.02.008
779 Campbell, G.H., Esser, K.M., and Weinbaum, F.I. (1977). Trypanosoma rhodesiense Infection
780 in B-Cell-Deficient Mice. Infection and Immunity *18*, 434–438.
781 Carrington, M., Miller, N., Blum, M., Roditi, I., Wiley, D., and Turner, M. (1991). Variant
782 Specific Glycoprotein of Trypanosoma brucei Consists of Two Domains each Having an
783 Independently Conserved Pattern of Cysteine Residues. J. Mol. Biol *221*, 823–835.
784 10.1016/0022-2836(91)80178-w
785 Correa, A.R.V., Berbel, A.C.E.R., Papa, M.P., de Morais, A.T.S., Peçanha, L.M.T., and de
786 Arruda, L.B. (2015). Dengue virus directly stimulates Polyclonal B cell activation. PLoS ONE
787 *10*. 10.1371/journal.pone.0143391
788 Cross, G.A.M. (1975). Identification, purification and properties of clone-specific glycoprotein
789 antigens constituting the surface coat of Trypanosoma brucei. Parasitology *71*, 393–417.
790 10.1017/S003118200004717X
791 Cross, G.A.M. (1984). Release and Purification of Trypanosoma brucei Variant Surface
792 Glycoprotein. Journal of Cellular Biochemistry *24*, 79–90. 10.1002/jcb.240240107
793 Diffley, P. (1983). Trypanosomal surface coat variant antigen causes polyclonal lymphocyte
794 activation. J Immunol. *131*, 1983–1986.
795 Fecher-Trost, C., Wissenbach, U., Beck, A., Schalkowsky, P., Stoerger, C., Doerr, J., Dembek,
796 A., Simon-Thomas, M., Weber, A., Wollenberg, P., et al. (2013). The in vivo TRPV6 protein
797 starts at a non-AUG triplet, decoded as methionine, upstream of canonical initiation at AUG.
798 Journal of Biological Chemistry *288*, 16629–16644. 10.1074/jbc.M113.469726
799 Freymann, D., Down, J., Carrington, M., Roditi, I., Turner, M., and Wiley, D. (1990). 2.9 A
800 Resolution Structure of the N-terminal Domain of a Variant Surface Glycoprotein from
801 Trypanosoma brucei. J. Mol. Biol *216*, 141–160. 10.1016/S0022-2836(05)80066-X

802 Grünfelder, C.G., Engstler, M., Weise, F., Schwarz, H., Stierhof, Y.-D., Boshart, M., and
803 Overath, P. (2002). Accumulation of a GPI-Anchored Protein at the Cell Surface Requires
804 Sorting at Multiple Intracellular Levels. Traffic *3*, 547–559. 10.1034/j.1600-
805 0854.2002.30805.x
806 Hall, J.P.J., Wang, H., and David Barry, J. (2013). Mosaic VSGs and the Scale of Trypanosoma
807 brucei Antigenic Variation. PLoS Pathogens *9*. 10.1371/journal.ppat.1003502
808 Hempelmann, A., Hartleb, L., van Straaten, M., Hashemi, H., Zeelen, J.P., Bongers, K.,
809 Papavasiliou, F.N., Engstler, M., Stebbins, C.E., and Jones, N.G. (2021). Nanobody-mediated
810 macromolecular crowding induces membrane fission and remodeling in the African
811 trypanosome. Cell Reports *37*. 10.1101/2021.01.13.426364
812 Hirumi, H., and Hirumi, K. (1989). Continuous Cultivation of Trypanosoma brucei Blood
813 Stream Forms in a Medium Containing a Low Concentration of Serum Protein without Feeder
814 Cell Layers. The Journal of Parasitology *75*, 985–989.
815 Holm, L. (2020). DALI and the persistence of protein shape. Protein Science *29*, 128–140.
816 0.1002/pro.3749
817 Jayaraman, S., Harris, C., Paxton, E., Donachie, A.M., Vaikkinen, H., McCulloch, R., Hall,
818 J.P.J., Kenny, J., Lenzi, L., Hertz-Fowler, C., et al. (2019). Application of long read sequencing
819 to determine expressed antigen diversity in Trypanosoma brucei infections. PLoS Neglected
820 Tropical Diseases *13*. 10.1371/journal.pntd.0007262
821 Lee, J., Boutz, D.R., Chromikova, V., Joyce, M.G., Vollmers, C., Leung, K., Horton, A.P.,
822 DeKosky, B.J., Lee, C.H., Lavinder, J.J., et al. (2016). Molecular-level analysis of the serum
823 antibody repertoire in young adults before and after seasonal influenza vaccination. Nature
824 Medicine *22*, 1456–1464. 10.1038/nm.4224
825 Lee, J., Paparoditis, P., Horton, A.P., Frühwirth, A., McDaniel, J.R., Jung, J., Boutz, D.R.,
826 Hussein, D.A., Tanno, Y., Pappas, L., et al. (2019). Persistent Antibody Clonotypes Dominate

827 the Serum Response to Influenza over Multiple Years and Repeated Vaccinations. Cell Host
828 and Microbe *25*, 367-376.e5. 10.1016/j.chom.2019.01.010
829 Lisowska, E. (2002). The role of glycosylation in protein antigenic properties. CMLS, Cell.
830 Mol. Life Sci *59*, 445–455. 10.1007/s00018-002-8437-3
831 Manthri, S., Güther, M.L.S., Izquierdo, L., Acosta-serrano, A., and Ferguson, M.A.J. (2008).
832 Deletion of the TbALG3 gene demonstrates site-specific N-glycosylation and N-glycan
833 processing in Trypanosoma brucei. Glycobiology *18*, 367–383. 10.1093/glycob/cwn014
834 Marty, M.T., Baldwin, A.J., Marklund, E.G., Hochberg, G.K.A., Benesch, J.L.P., and
835 Robinson, C. v. (2015). Bayesian deconvolution of mass and ion mobility spectra: From binary
836 interactions to polydisperse ensembles. Analytical Chemistry *87*, 4370–4376.
837 10.1021/acs.analchem.5b00140
838 Mehlert, A., Richardson, J.M., and Ferguson, M.A.J. (1998). Structure of the
839 Glycosylphosphatidylinositol Membrane Anchor Glycan of a Class-2 Variant Surface
840 Glycoprotein from Trypanosoma brucei. Journal of Molecular Biology *277*, 379–392.
841 10.1006/jmbi.1997.1600
842 Metcalf, P., Blum, M., Freymann, D., Turner, M., and Wiley, D.C. (1987). Two Variant Surface
843 Glycoproteins of Trypanosoma brucei of different sequence classes have similar 6A resolution
844 X-ray structures. Nature *325*, 84–86. 10.1038/325084a0
845 Moir, S., and Fauci, A.S. (2009). B cells in HIV infection and disease. Nature Reviews
846 Immunology *9*, 235–245. 10.1038/nri2524
847 Mugnier, M.R., Cross, G.A.M., and Papavasiliou, F.N. (2015). The in vivo dynamics of
848 antigenic variation in Trypanosoma brucei. Science *347*, 1470–1473. 10.1126/science.aaa4502
849 Müller, N., Mansfield, J.M., and Seebeck, T. (1996). Trypanosome Variant Surface
850 Glycoproteins Are Recognized by Self-Reactive Antibodies in Uninfected Hosts. Infection and
851 Immunity *64*, 4593–4597. 10.1128/iai.64.11.4593-4597.1996

852 Paul Dominic B. Olinares, and Brian T. Chait (2020). Native Mass Spectrometry Analysis of
853 Affinity-Captured Endogenous Yeast RNA Exosome Complexes. In The Eukaryotic RNA
854 Exosome, Methods and Protocols Methods in Molecular Biology, (Clifton, N.J.), pp. 357–382.
855 10.1007/978-1-4939-9822-7_17
856 Pinger, J., Chowdhury, S., and Papavasiliou, F.N. (2017). Variant surface glycoprotein density
857 defines an immune evasion threshold for African trypanosomes undergoing antigenic variation.
858 Nature Communications *8*. 10.1038/s41467-017-00959-w
859 Pinger, J., Nešić, D., Ali, L., Aresta-Branco, F., Lilic, M., Chowdhury, S., Kim, H.S., Verdi, J.,
860 Raper, J., Ferguson, M.A.J., et al. (2018). African trypanosomes evade immune clearance by
861 O-glycosylation of the VSG surface coat. Nature Microbiology *3*, 932–938. 10.1038/s41564-
862 018-0187-6
863 Pracht, K., Meinzinger, J., Daum, P., Schulz, S.R., Reimer, D., Hauke, M., Roth, E., Mielenz,
864 D., Berek, C., Côrte-Real, J., et al. (2017). A new staining protocol for detection of murine
865 antibody-secreting plasma cell subsets by flow cytometry. European Journal of Immunology
866 *47*, 1389–1392. 10.1002/eji.201747019
867 Reid, D.J., Diesing, J.M., Miller, M.A., Perry, S.M., Wales, J.A., Montfort, W.R., and Marty,
868 M.T. (2019). MetaUniDec: High-Throughput Deconvolution of Native Mass Spectra. Journal
869 of the American Society for Mass Spectrometry *30*, 118–127. 10.1007/s13361-018-1951-9
870 Scheid, J.F., Mouquet, H., Feldhahn, N., Walker, B.D., Pereyra, F., Cutrell, E., Seaman, M.S.,
871 Mascola, J.R., Wyatt, R.T., Wardemann, H., et al. (2009). A method for identification of HIV
872 gp140 binding memory B cells in human blood. Journal of Immunological Methods *343*, 65–
873 67. 10.1016/j.jim.2008.11.012
874 Silva-Barrios, S., Charpentier, T., and Stäger, S. (2018). The Deadly Dance of B Cells with
875 Trypanosomatids. Trends in Parasitology *34*, 155–171. 10.1016/j.pt.2017.10.001

876 Stijlemans, B., Radwanska, M., Trez, C. de, and Magez, S. (2017). African trypanosomes
877 undermine humoral responses and vaccine development: Link with inflammatory responses?
878 Frontiers in Immunology *8*. 10.3389/fimmu.2017.00582
879 Tiller, T., Meffre, E., Yurasov, S., Tsuiji, M., Nussenzweig, M.C., and Wardemann, H. (2008).
880 Efficient generation of monoclonal antibodies from single human B cells by single cell RT-
881 PCR and expression vector cloning. Journal of Immunological Methods *329*, 112–124.
882 10.1016/j.jim.2007.09.017
883 Triller, G., Scally, S.W., Costa, G., Pissarev, M., Kreschel, C., Bosch, A., Marois, E., Sack,
884 B.K., Murugan, R., Salman, A.M., et al. (2017). Natural Parasite Exposure Induces Protective
885 Human Anti-Malarial Antibodies. Immunity *47*, 1197-1209.e10.
886 10.1016/j.immuni.2017.11.007
887 Verdi, J., Zipkin, R., Hillman, E., Gertsch, R.A., Pangburn, S.J., Thomson, R., Papavasiliou,
888 N., Sternberg, J., and Raper, J. (2020). Inducible Germline IgMs Bridge Trypanosome Lytic
889 Factor Assembly and Parasite Recognition. Cell Host and Microbe *28*, 79-88.e4.
890 10.1016/j.chom.2020.04.012
891 de Vita, S., Quartuccio, L., and Fabris, M. (2008). Hepatitis C virus infection, mixed
892 cryoglobulinemia and BLyS upregulation: Targeting the infectious trigger, the autoimmune
893 response, or both? Autoimmunity Reviews *8*, 95–99. 10.1016/j.autrev.2008.05.005
894 Waickman, A.T., Gromowski, G.D., Rutvisuttinunt, W., Li, T., Siegfried, H., Victor, K.,
895 Kuklis, C., Gomootsukavadee, M., McCracken, M.K., Gabriel, B., et al. (2020). Transcriptional
896 and clonal characterization of B cell plasmablast diversity following primary and secondary
897 natural DENV infection. EBioMedicine *54*. 10.1016/j.ebiom.2020.102733
898 Woods, A., Monneaux, F., Soulas-Sprauel, P., Muller, S., Martin, T., Korganow, A.-S., and
899 Pasquali, J.-L. (2007). Influenza Virus-Induced Type I Interferon Leads to Polyclonal B-Cell
900 Activation but Does Not Break Down B-Cell Tolerance. Journal of Virology *81*, 12525–12534.
901 10.1128/jvi.00839-07

902 Ye, J., Ma, N., Madden, T.L., and Ostell, J.M. (2013). IgBLAST: an immunoglobulin variable
903 domain sequence analysis tool. Nucleic Acids Research *41*, W34–W40. 10.1093/nar/gkt382
904 Zamze, S.E., Ashford, D.A., Wooten, E.W., Rademacher, T.W., and Dwek, R.A. (1991).
905 Structural characterization of the asparagine-linked oligosaccharides from Trypanosoma brucei
906 Type II and Type III variant surface glycoproteins. Journal of Biological Chemistry *266*,
907 20244–20261. 10.1016/s0021-9258(18)54916-4
908 Zoll, S., Lane-Serff, H., Mehmood, S., Schneider, J., Robinson, C. v., Carrington, M., and
909 Higgins, M.K. (2018). The structure of serum resistance-associated protein and its implications
910 for human African trypanosomiasis. Nature Microbiology *3*, 295–301. 10.1038/s41564-017-
911 0085-3